Supplementary Information (SI) for Journal of Materials Chemistry A.
This journal is © The Royal Society of Chemistry 2026

Supplementary Information (SI)

Interfacial Electron Transfer-Driven Activity Enhancements of Carbide/Alloy Heterostructured Catalysts toward Water Electrolysis for High-Performance Anion Exchange Membrane Water Electrolysis

Kai-An Lee,[a] Yu-Chieh Ting, [a] Chiung-Wen Chang, [a] Tzu-Hsiang Lin, [a] Shao-I Chang, [a] Tsung-Wei Hsueh, [a] Chia-Hsien Lin,[a] Shih-Yuan Lu[a]*

[a] Department of Chemical Engineering, National Tsing Hua University, Hsinchu 300044, Taiwan
*Email: sylu@mx.nthu.edu.tw

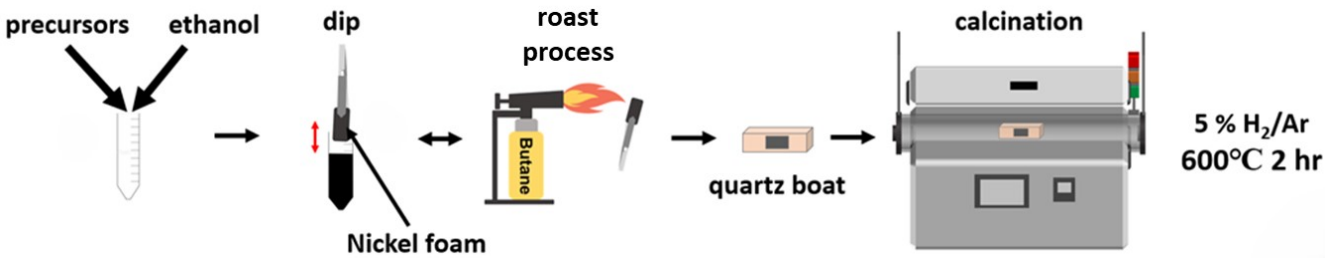

Scheme S1. Illustration of fabrication process for carbide/alloy heterostructured catalysts.

Table S1. Metallic compositions of sample catalysts determined with ICP-OES.

	Fe (at%)	Ni (at%)	Mo (at%)
Mo_2C/NiMo	-	54.3	45.7
Mo_2C/FeNiMo	15.9	48.1	35.9
Mo_2C	-	-	100.0*
NiMo	-	89.8	10.2
FeNiMo	21.0	68.8	10.2

*: exclude Ni contamination.

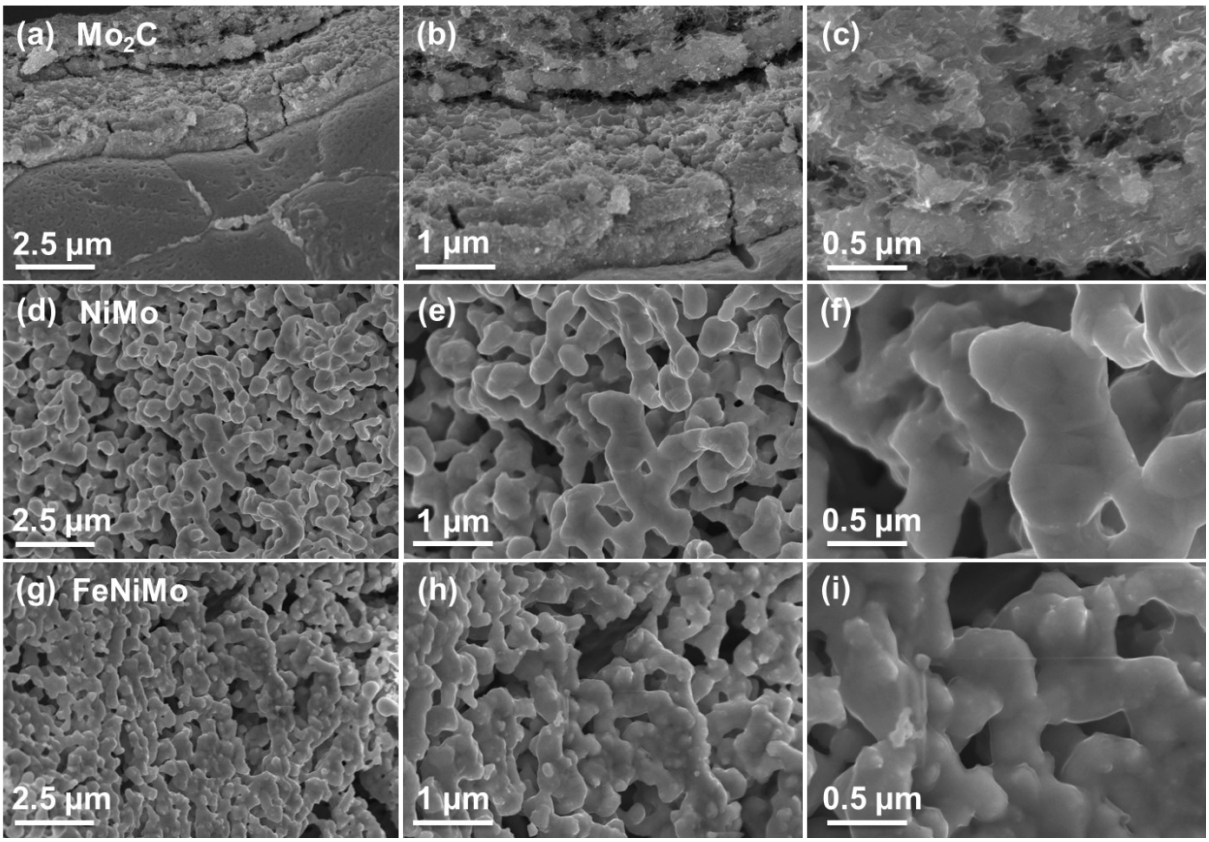

Figure S1. SEM images of (a-c) Mo_2C, (d-f) NiMo, and (g-i) FeNiMo at increasing magnifications.

Table S2. Binding energies of constituent peaks of Ni 2p in HRXPS spectra of Mo_2C/NiMo and NiMo.

		Ni^0 (eV)	Ni^{2+} (eV)	sat. (eV)
Mo_2C/NiMo	Ni $2p_{3/2}$	870.3	873.4	877.4
	Ni $2p_{1/2}$	853.0	856.1	860.1
NiMo	Ni $2p_{3/2}$	870.2	873.3	877.3
	Ni $2p_{1/2}$	852.9	856.0	860.0

Table S3. Binding energies of constituent peaks of C 1s in HRXPS spectra of Mo_2C/NiMo and Mo_2C.

	C=O (eV)	C-O (eV)	C-C/C-H (eV)	Mo-C (eV)
Mo_2C/NiMo	288.4	285.7	284.8	284.2
Mo_2C	288.4	285.7	284.8	284.2

Table S4. Binding energies of constituent peaks of Mo 3d in HRXPS spectra of Mo_2C/NiMo, Mo_2C, and NiMo.

		Mo^0 (eV)	Mo^{2+} (eV)	Mo^{4+} (eV)	Mo^{6+} (eV)
Mo_2C/NiMo	Mo $3d_{3/2}$	231.2	231.4	232.5	235.3
	Mo $3d_{5/2}$	228.0	228.3	229.3	232.1
Mo_2C	Mo $3d_{3/2}$	-	231.5	232.6	235.5
	Mo $3d_{5/2}$	-	228.4	229.4	232.2
NiMo	Mo $3d_{3/2}$	231.3	-	232.6	235.4
	Mo $3d_{5/2}$	228.1	-	229.4	232.2

Table S5. Binding energies of constituent peaks of Fe 2p in HRXPS spectra of Mo_2C/FeNiMo and FeNiMo.

		Fe^0 (eV)	Fe^{2+} (eV)	Fe^{3+} (eV)	sat. (eV)
Mo_2C/FeNiMo	Fe $2p_{3/2}$	720.5	723.4	725.6	728.5
	Fe $2p_{1/2}$	707.4	710.3	712.5	715.4
FeNiMo	Fe $2p_{3/2}$	720.4	723.3	725.5	728.4
	Fe $2p_{1/2}$	707.3	710.2	712.4	715.3

Table S6. Binding energies of constituent peaks of Ni 2p in HRXPS spectra of Mo_2C/FeNiMo and FeNiMo.

		Ni^0 (eV)	Ni^{2+} (eV)	sat. (eV)
Mo_2C/FeNiMo	Ni $2p_{3/2}$	870.3	873.4	877.4
	Ni $2p_{1/2}$	853.0	856.1	860.1
FeNiMo	Ni $2p_{3/2}$	870.2	873.3	877.3
	Ni $2p_{1/2}$	852.9	856.0	860.0

Table S7. Binding energies of constituent peaks of C 1s in HRXPS spectra of Mo_2C/FeNiMo and Mo_2C.

	C=O (eV)	C-O (eV)	C-C (eV)	Mo-C (eV)
Mo_2C/FeNiMo	288.4	286.0	284.6	284.2
Mo_2C	288.4	285.7	284.8	284.2

Table S8. Binding energies of constituent peaks of Mo 3d in HRXPS spectra of Mo_2C/NiMo, Mo_2C and NiMo.

		Mo^0 (eV)	Mo^{2+} (eV)	Mo^{4+} (eV)	Mo^{6+} (eV)
Mo_2C/FeNiMo	Mo $3d_{3/2}$	231.2	231.4	232.5	235.3
	Mo $3d_{5/2}$	228.0	228.3	229.3	232.1
Mo_2C	Mo $3d_{3/2}$	-	231.5	232.6	235.5
	Mo $3d_{5/2}$	-	228.4	229.4	232.2
FeNiMo	Mo $3d_{3/2}$	231.3	-	232.6	235.4
	Mo $3d_{5/2}$	228.1	-	229.4	232.2

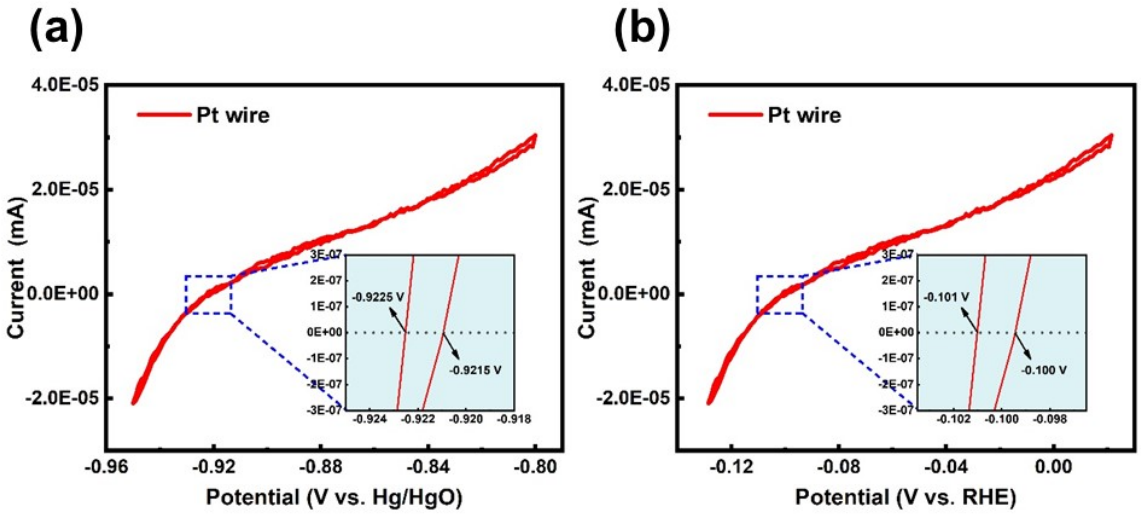

Figure S2. The reference electrode is calibrated in a three-electrode system, with Pt wires serving as both working and counter electrodes and Hg/HgO as the reference electrode in 1.0 M KOH. The pH value of the electrolyte is determined to be 13.9 with a pH meter. Prior to the calibration, the electrolyte is saturated with H_2 for at least 30 mins. The scan rate is set at 1.0 mV s^{-1}. The potential of Hg/HgO is calibrated by aligning the average of the zero current potential (-0.922 vs. Hg/HgO) of the CV curve (inset of **Figure S2a**) to 0 V vs. RHE (inset of **Figure S2b**) according to Nernst's equation ($E_{RHE} = E_{Hg/HgO} + 0.0591 \times pH + E^0_{Hg/HgO}$). Consequently, the potential of the reference electrode used in this work is calibrated to 0.1005 V (vs. NHE).

Table S9. Charge transfer resistances (R_{ct}) of HER catalyzed by sample catalysts determined at -0.2 V (vs. RHE).

Catalyst	R_{ct} (Ω)
Mo_2C/NiMo	0.94
Mo_2C	1.00
NiMo	4.35

Table S10. Charge transfer resistances (R_{ct}) of OER catalyzed by sample catalysts determined at 1.53 V (vs. RHE).

Catalyst	R_{ct} (Ω)
Mo_2C/FeNiMo	1.05
Mo_2C	1.70
FeNiMo	2.03

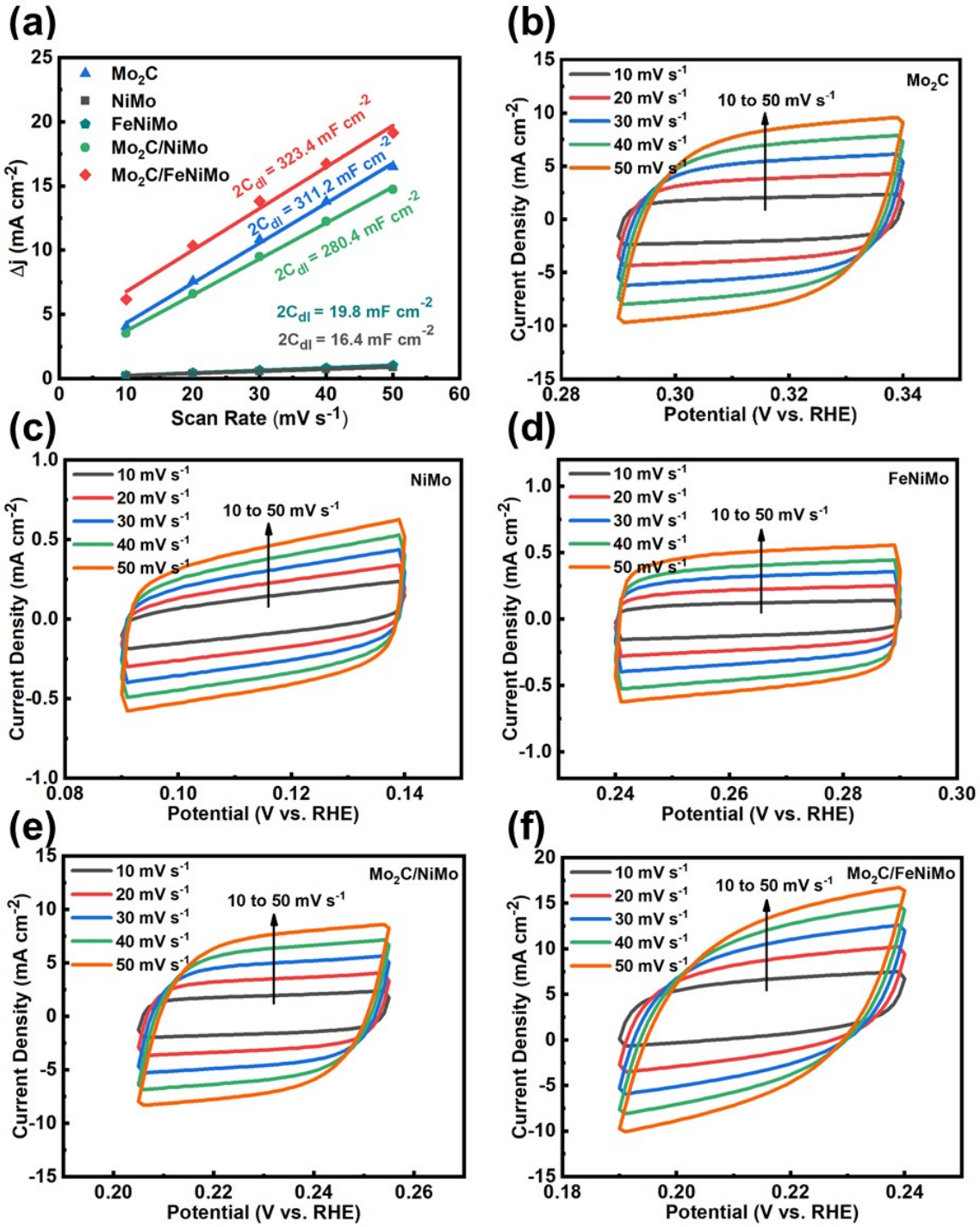

Figure S3. (a) Linear fitting of current density differences ($\Delta j = j_a - j_c$) at a specific potential versus scan rates for determination of electric double layer capacitances (C_{dl}) of sample catalysts as halves of obtained slopes. Cyclic voltammetry curves recorded at increasing scan rates in 1 M KOH for: (b) Mo_2C, (c) NiMo, (d) FeNiMo, (e) Mo_2C/NiMo, and (f) Mo_2C/FeNiMo.

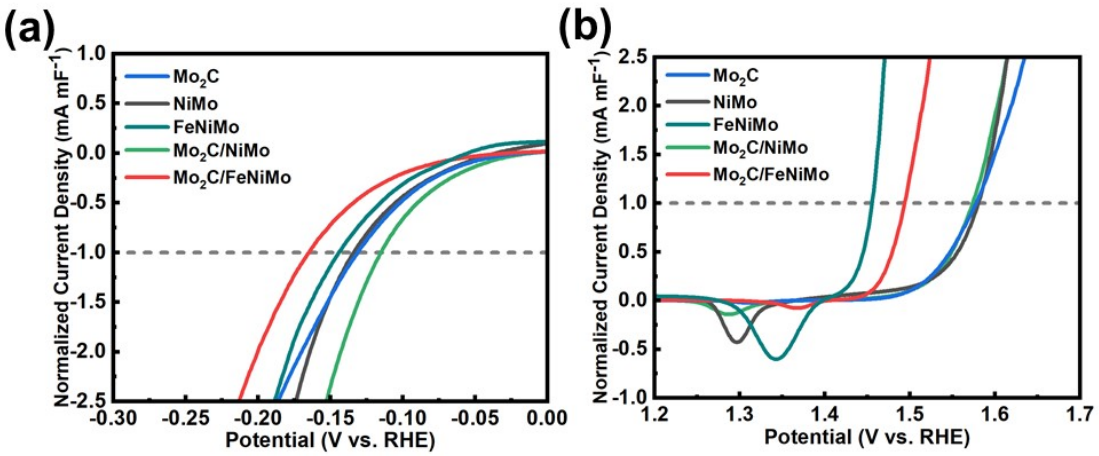

Figure S4. C_{dl}-normalized polarization curves for (a) HER and (b) OER catalyzed by sample catalysts.

Table S11. Electrochemical performances of Mo_2C/NiMo//PiperION//Mo_2C/FeNiMo based AEMWE compared with those of state-of-the-art non-precious transition metal catalysts based AEMWE's reported in recent years.

Cathode	Membrane	Anode	Electrolyte	Cell temperature (℃)	Current density	Ref.
Mo_2C/NiMo@NF	**PiperION**	**Mo_2C/FeNiMo@NF**	**1 M KOH**	**60**	**2645 mA cm^{-2} @2.0V**	**This work**
Mo_5N_6/Ni-450	FAA-3-PK-130	Mo_5N_6/Co-450	1 M KOH	70	450 mA cm^{-2} @1.8V	[1]
PMoNiTm	UTP220	NiFe LDH	1 M KOH	70	520 mA cm^{-2} @2.0V	[2]
BP/$CoNiSe_2$	FAA-3-50	NiFe LDH	1 M KOH	60	600 mA cm^{-2} @1.9V	[3]
NiFeS@Ti_3C_2	X37-50 RT	NiFeS@Ti_3C_2	1 M KOH	50	800 mA cm^{-2} @2.0V	[4]
$Ce_{0.1}$-Fe_2P/NiCoP	X37-50	$Ce_{0.1}$-Fe_2P/NiCoP	1 M KOH	60	900 mA cm^{-2} @1.8V	[5]
$NiMoO_x$@CMK-3	FAA-3-50	NiFe LDH	1 M KOH	50	1140 mA cm^{-2} @2.0V	[6]
Co_2P-NiP_5/NF	FAA-3-50	Fe_2P-$Ni_{12}P_5$/NF	1 M KOH	60	1200 mA cm^{-2} @2.0V	[7]
Ni-CeO_2/Carbon	HQPC-TMA	Co_3O_4	alkaline	60	1500 mA cm^{-2} @2.0V	[8]
Mn-NiFe@WO_x	PiperION	Mn-NiFe@WO_x	1 M KOH	60	1600 mA cm^{-2} @2.0V	[9]

Table S12. High frequency resistance (HFR) and charge transfer resistances (R_1 for HER and R_2 for OER) of sample AEMWE's determined at 1.8 V.

AEMWE	EIS measurements		
	HFR	R_1 (HER)	R_2 (OER)
Mo_2C/NiMo@N//PiperION//Mo_2C/FeNiMo@NF	0.019	0.0110	0.0145
Mo_2C@NF//PiperION//Mo_2C/FeNiMo@NF	0.022	0.0113	0.0145
Mo_2C/NiMo@NF//PiperION//FeNiMo@NF	0.021	0.0110	0.0209
Mo_2C/NiMo@NF//PiperION//Mo_2C@NF	0.022	0.0110	0.0518
NiMo@NF//PiperION//Mo_2C/FeNiMo@NF	0.023	0.0655	0.0145

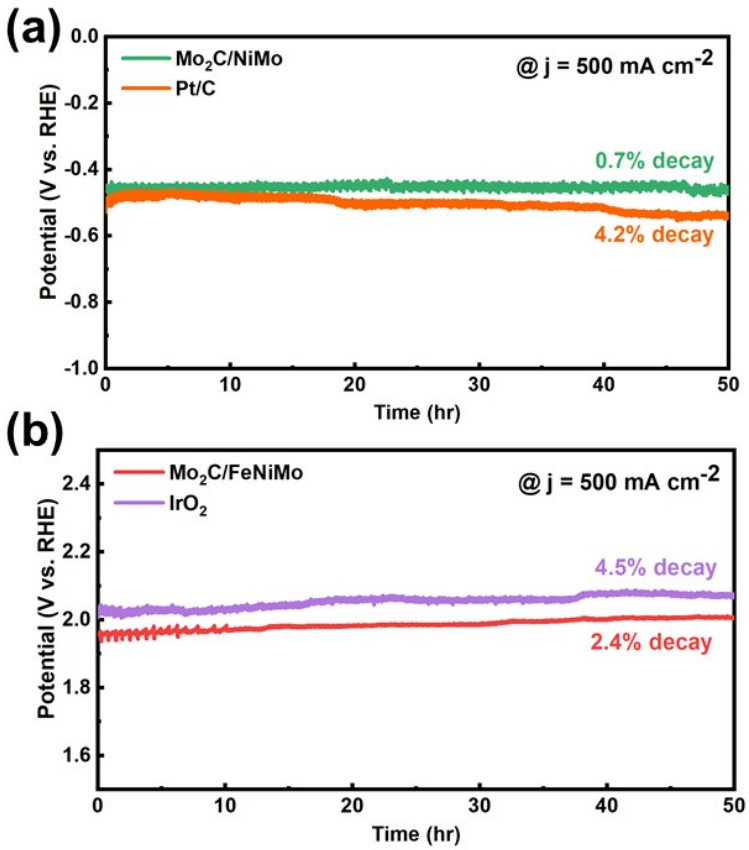

Figure S5. Chronopotentiometric stability tests for (a) Mo_2C/NiMo and (b) Mo_2C/FeNiMo under 0.5 A cm^{-2} for 50 hours toward HER and OER operations, respectively.

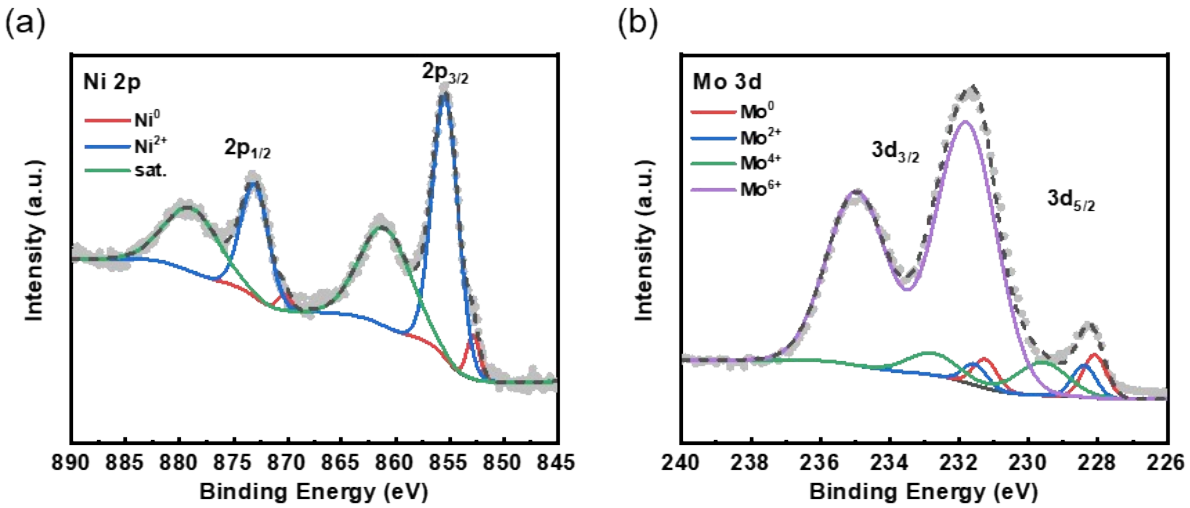

Figure S6. HRXPS spectra of (a) Ni 2p and (c) Mo 3d for Mo_2C/NiMo after HER stability test.

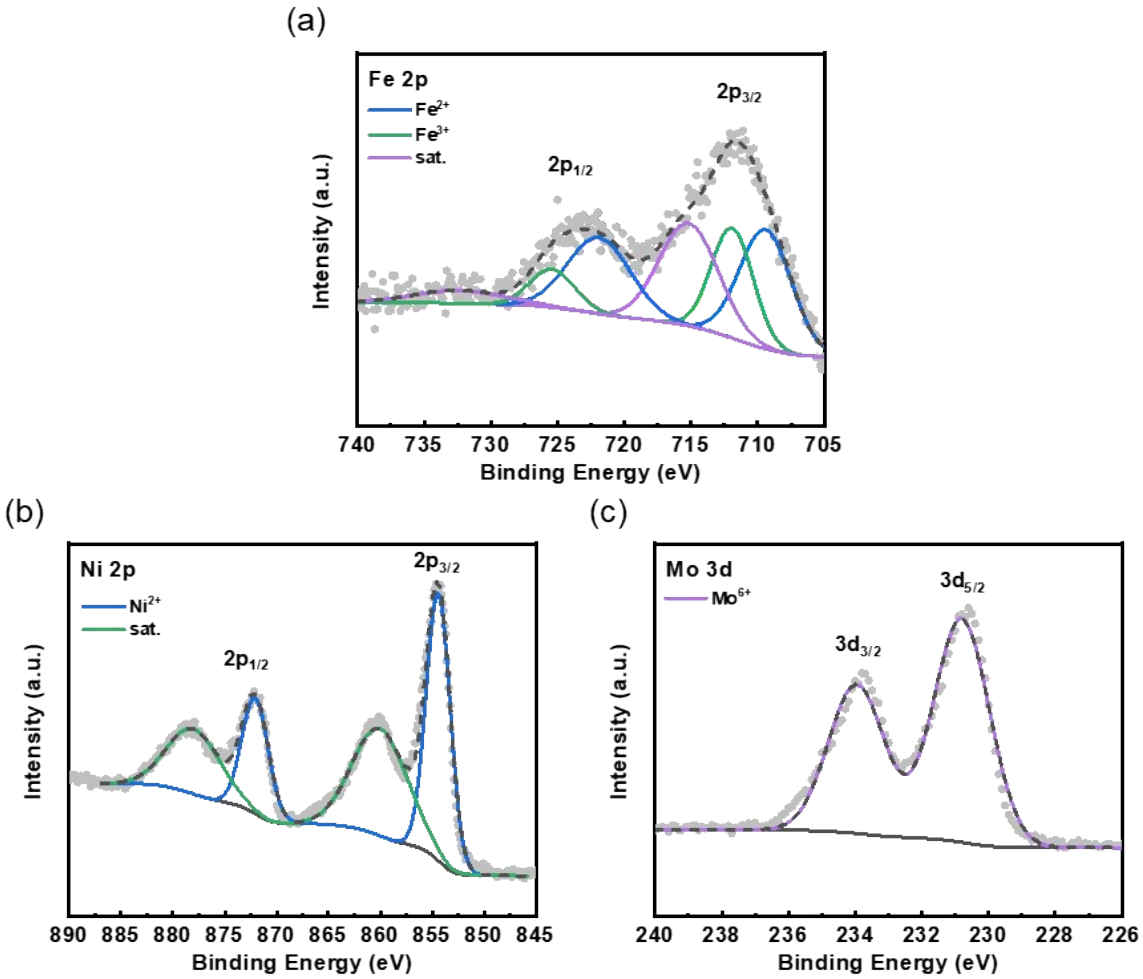

Figure S7. HRXPS spectra of (a) Fe 2p, (b) Ni 2p, and (c) Mo 3d for Mo_2C/FeNiMo after OER stability test.

Table S13. Ratio of $(Ni^{0}+Mo^{0}+Mo^{2+})/(Ni^{0}+Ni^{2+}+Mo^{0}+Mo^{2+}+Mo^{4+}+Mo^{6+})$ for Mo_2C/NiMo before and after HER stability test.

	Ni	Mo
Mo_2C/NiMo	A/B (%)	A/B (%)
before	11.5	26.7
after	7.5	9.2

Table S14. Ratio of $(Fe^{0}+Ni^{0}+Mo^{0}+Mo^{2+})/(Fe^{0}+Fe^{2+}+Fe^{3+}+Ni^{0}+Ni^{2+}+Mo^{0}+Mo^{2+}+Mo^{4+}+Mo^{6+})$ for Mo_2C/FeNiMo before and after OER stability test.

	Fe	Ni	Mo
Mo_2C/FeNiMo	A/B (%)	A/B (%)	A/B (%)
before	12.0	18.3	27.6
after	0.0	0.0	0.0

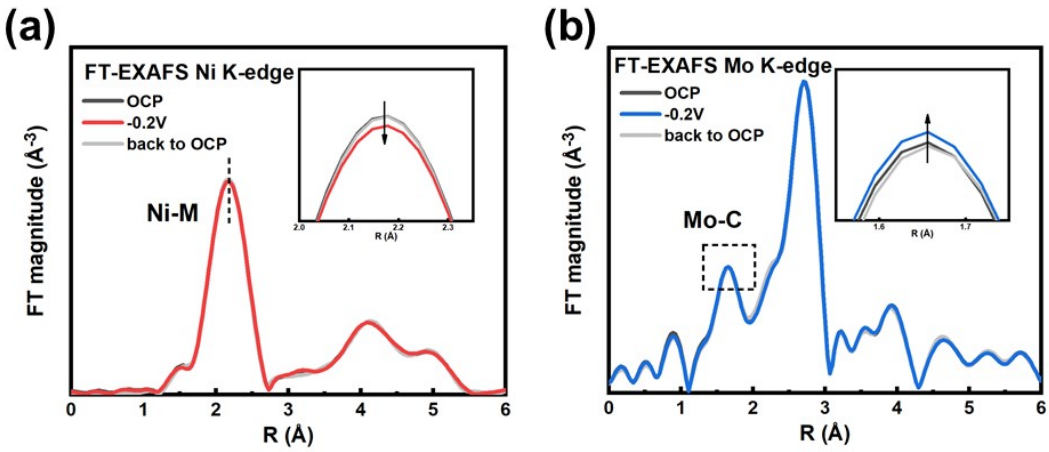

Figure S8. In-situ FT-EXAFS spectra of Mo_2C/NiMo under cathodic condition at (a) Ni K-edge and (b) Mo K-edge. Insets show corresponding locally enlarged overlaid curves.

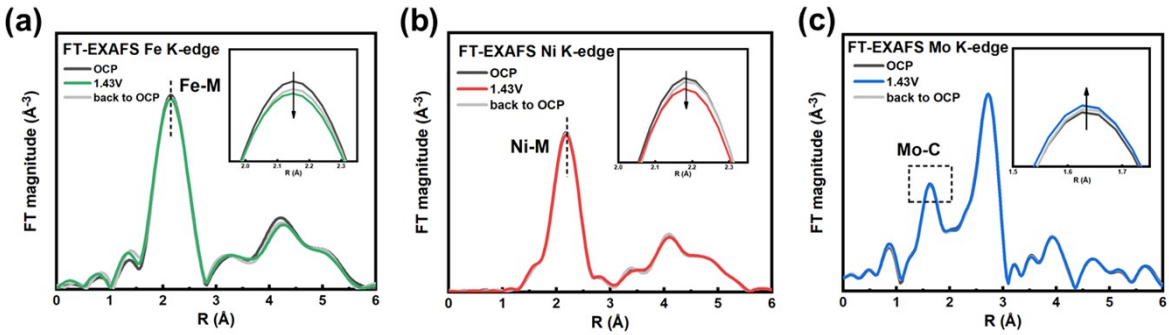

Figure S9. In-situ FT-EXAFS spectra of Mo_2C/FeNiMo under anodic condition at (a) Fe K-edge, (b) Ni K-edge, and (c) Mo K-edge. Insets show corresponding locally enlarged overlaid curves.

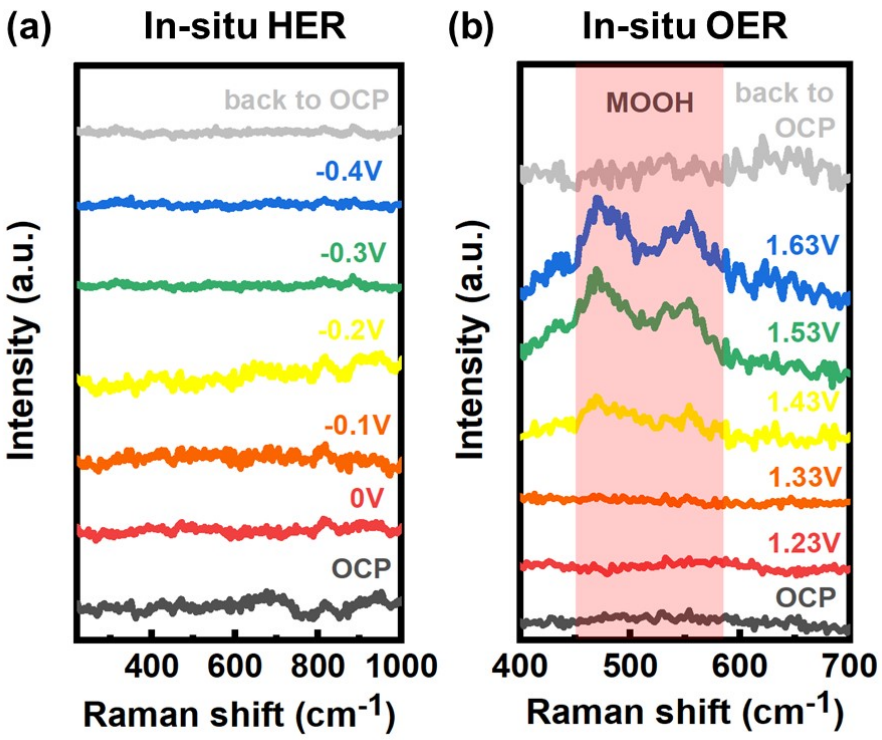

Figure S10. In-situ Raman spectra of (a) Mo_2C/NiMo under HER conditions and (b) Mo_2C/FeNiMo under OER conditions.

References

[S1] Dong YM, Wu AP, Yang GC, Wang JQ, Liu Y, Yan HJ, et al., Lower-Temperature Synthesis of Nitrogen-Rich Molybdenum Nitride/Nickel (Cobalt) Heterojunctional Assembly for the Effective Water Electrolysis, *Advanced Functional Materials*, 2025; 35: 2412979.

[S2] Zhou T, Yu S, Tang YQ, Huang XT, Fu JJ, Shen PK, et al., Built-in electric field engineering of MoO_2-Ni heterostructure by P_{3p}-Mo_{4d}-Tm_{4f} orbitals hybridization for efficient industrial-level hydrogen production, *Chemical Engineering Journal*, 2025; 508: 160921 .

[S3] Wen T, Zheng Y, Wang HT, Zou J, Constructing black phosphorus nanosheet/$CoNiSe_2$ nanoflower heterojunction with effective built-in electric field for robust H_2 evolution in anion exchange membrane water electrolyzer, *Applied Catalysis B-Environment and Energy*, 2025; 378: 125588.

[S4] Chanda D, Kannan K, Gautam J, Meshesha MM, Jang SG, Dinh V, et al., Effect of the interfacial electronic coupling of nickel-iron sulfide nanosheets with layer Ti_3C_2 MXenes as efficient bifunctional electrocatalysts for anion-exchange membrane water electrolysis, *Applied Catalysis B-Environment and Energy*, 2023; 321: 122039.

[S5] Zhang F, Wang K, Zhang H, Yang SL, Xu M, He Y, et al., Dynamic Reconstruction of Ce-Doped Fe_2P/NiCoP Hybrid for Ampere-Level Oxygen Evolution in Anion Exchange Membrane Water Electrolysis, *Advanced Functional Materials*, 2025; 35: 2500861.

[S6] Chen YH, Yue KH, Zhao JW, Cai ZY, Wang XY, Yan Y, Effective modulating of the Mo dissolution and polymerization in $Ni_4Mo/NiMoO_4$ heterostructure via metal-metal oxide-support interaction for boosting H_2 production, *Chemical Engineering Journal*, 2023; 466: 143097.

[S7] Guo L, Liu XY, He ZX, Chen ZC, Zhang ZY, Pan L, et al., Self-Supported Bimetallic Phosphide Heterojunction-Integrated Electrode Promoting High-Performance Alkaline Anion-Exchange Membrane Water Electrolysis, *ACS Sustain Chem Eng*, 2022; 10: 9956-68.

[S8] Kim NI, Lee J, Jin S, Jeong J, Myeong SW, Ha JS, et al., Collapsing the Bottleneck by Interfacial Effect of Ni/CeO for Long-Term Hydrogen Production using Waste Alkaline Water in Practical-Scale Anion Exchange Membrane Water Electrolyzer, *Adv Sci*, 2025; 12: e02484.

[S9] Oh S, Roh H, Im H, Seo O, Takagi Y, Watanabe T, et al., Mn doped hierarchical water splitting electrocatalyst: Synthesis, surface analysis and application to AEMWE, *Chemical Engineering Journal*, 2024; 500: 157106.